Published in final edited form as:
New J Phys. 2010 July ; 12: . doi:10.1088/1367-2630/12/7/073011.

Design of an electron microscope phase plate using a focused continuous-wave laser

H Müller[1,7], **Jian Jin**[2], **R Danev**[3], **J Spence**[4], **H Padmore**[5], and **R M Glaeser**[6]

[1]Physics Department, University of California, Berkeley, CA 94720, USA

[2]Engineering Division, Lawrence Berkeley National Laboratory, University of California, Berkeley, CA 94720, USA

[3]Division of Nano-Structure Physiology, Okazaki Institute for Integrative Bioscience, 5-1 Higashiyama, Myodaiji, Okazaki 444-8787, Japan

[4]Physics Department, Arizona State University, Tempe, AZ 85287-1504, USA

[5]Advanced Light Source, Lawrence Berkeley National Laboratory, University of California, Berkeley, CA 94720, USA

[6]Life Sciences Division, Lawrence Berkeley National Laboratory, University of California, Berkeley, CA 94720, USA

Abstract

We propose a Zernike phase contrast electron microscope that uses an intense laser focus to convert a phase image into a visible image. We present the relativistic quantum theory of the phase shift caused by the laser–electron interaction, study resonant cavities for enhancing the laser intensity and discuss applications in biology, soft-materials science and atomic and molecular physics.

1. Introduction

The resolution of modern transmission electron microscopes (TEMs) [1] can be more than 10 000 times that of light microscopes. Yet, the imaging performance of TEMs for thin soft matter such as biological specimens is limited: these specimens are weakly scattering phase objects and a perfect image of them shows almost no contrast. The image is imprinted, however, on the phase of the electron's wave function. In optical microscopes, such a phase image can be made visible by Zernike phase contrast microscopy [2]: the part of the light beam that has not been diffracted by the specimen is phase shifted by $\pi/2$ by a quarter-wave plate, thus converting phase modulation into visible amplitude modulation.

Quarter-wave plates for TEMs have been suggested early [3] but could not be fabricated until recently. Examples are thin carbon film phase plates [4,5], electrostatic (einzel lens) designs [6,7] or thin bar magnets [8]. Although the most recent implementations are greatly improved over earlier versions [9], they are still prone to becoming electrostatically charged when they are hit by an electron beam. This causes distortion of the image. While it ought to be possible to overcome this limitation by using suitable materials and by keeping the surface of devices extremely clean, such solutions are not necessarily well suited for routine TEM applications. Moreover, microfabricated phase plates induce electron loss, leading to reduced performance.

[7]Author to whom any correspondence should be addressed. hm@berkeley.edu.

Attempts have also been made to use bi-prism electron holography to record the phase of the electron beam, but this approach has been largely abandoned because subtle charging effects in the specimen itself result in degraded temporal coherence in an off-axis hologram, whereas they have little effect on the in-line holography that is provided by Zernike phase-contrast imaging.

In view of these challenges, the phase shift that occurs when an electron passes through a beam of light [10] is here envisioned as an alternative way to achieve phase contrast. To provide the required high laser intensities, a pulsed laser can be used together with a synchronized pulsed TEM [11]. However, using a pulsed-source TEM introduces new constraints for routine TEM applications, e.g. lower averaged electron flux and thus longer data collection periods, as the electron density during a pulse cannot be higher than in continuous wave (cw) operation to avoid space charge effects and potentially greater complexity.

In this paper, we propose designs for a cw version of an optical-beam quarter-wave plate that we believe will be suitable for general use in a TEM. We will derive the phase shift of an electron wave and discuss implementations that reach the required small spot size and high intensity using focusing optics and optical cavities. Finally, we will discuss applications in biological specimens and other soft-matter specimens and give an outlook on other potential applications.

2. Origin of the phase shift

The phase shift of the electron wave function caused by the laser can be explained by the ponderomotive force, a repulsive force felt by electrons entering the electric field of a laser. It is given as [12] $\phi = \hbar\alpha\lambda\rho\delta t/m$, where $\hbar$ is the reduced Planck constant, α the fine structure constant, λ the laser wavelength, ρ the photon density, m the electron mass and δt the time interval. This is a nonrelativistic result. In the TEM however, the electron energy is comparable to mc^2 and thus relativistic corrections may be significant.

In order to obtain a relativistically correct result, we now derive the phase shift using the theory of quantum electrodynamics ([13], in particular sections 6 and 7). The electrons, long before the interaction with the laser, are described by a quantum state $|i\rangle$. A scattering matrix $S = 1 + S^{(1)} + S^{(2)} + \ldots$ describes the evolution of $|i\rangle$ into the final state $|f\rangle = S|i\rangle$, which we define long after the interaction. The first order $S^{(1)}$ describes emission or absorption of a single photon by an electron. This violates energy and momentum conservation, so $S^{(1)} = 0$. It is important for us that this still holds if the laser beam is focused: the electric field of the focused beam can be described in the momentum representation by a superposition of plane waves of various directions. Since $S^{(1)} = 0$ for each of these plane waves, regardless of their direction or polarization, it is also zero for the focused beam.

The leading nonzero effects are described by the second order, $S^{(2)}$. Most of these take place whether or not the electrons interact with the laser (e.g. annihilation, electron–electron scattering, self-energy and vacuum polarization [13]) and do not contribute to the phase shift of interest. The remaining process (figure 1), called Compton scattering, can transfer momentum and energy to the electron. The scattering rate for such a transfer is $r = \sigma_T\rho\upsilon$, where $\sigma_T = [\alpha\hbar/(mc^2)]^2$ is the Thomson cross section and υ the electron velocity. Since electrons whose momenta have changed do not contribute to the TEM image, Compton scattering with momentum transfer is a loss mechanism.

The desired phase shift is caused by Compton scattering in the case where the incoming and outgoing electrons have the same energy. We will call this process *stimulated* Compton scattering for reasons that will become obvious. From the Feynman diagrams in figure 1, the

scattering matrix S can be calculated by following the Feynman rules, see [13], chapter 7.3. If we define $\phi \equiv \langle f|S^{(2)}|i\rangle$, the result can be expressed as (using $\hbar = m = c = 1$)

$$\begin{aligned}\phi &= \frac{(2\pi)^4\delta^{(4)}(p_1+k_1-p_2-k_2)}{2V^2\sqrt{E_{p_1}E_{p_2}\omega_{k_1}\omega_{k_2}}}(S_A+S_B),\\ S_A &= -e^2\bar{u}(\vec{p}_2)\not{\varepsilon}(\vec{k}_2)\mathrm{i}S_F(q)\not{\varepsilon}(\vec{k}_1)u(\vec{p}_1)a^\dagger(\vec{k}_1)a(\vec{k}_2),\\ S_B &= -e^2\bar{u}(\vec{p}_2)\not{\varepsilon}(\vec{k}_1)\mathrm{i}S_F(q)\not{\varepsilon}(\vec{k}_2)u(\vec{p}_1)a^\dagger(\vec{k}_2)a(\vec{k}_1).\end{aligned} \quad (1)$$

Here S_A and S_B denote terms arising from figures 1(A) and (B). Here, $\delta^{(4)}$ is the four-dimensional Dirac delta function, V the normalization volume, E_p the energy of an electron of four-momentum p, ω_k the photon frequency, S_F the Feynman propagator [13] and u and $\not{\varepsilon}$ describe electron and photon polarization, respectively. Since no momentum is transferred, $\vec{k}_1 = \vec{k}_2$, and we identify $\rho \equiv a^\dagger(\vec{k}_1)a(\vec{k}_1)/V$ as the photon density operator. Physically, this means that the emission of the outgoing photon is stimulated by the laser (hence the name), in contrast to the *spontaneous* case that is treated in most textbooks. We obtain [13][8] $\phi = -[\mathrm{i}e^2\rho/(2E_p\omega)]\bar{u}(\vec{p})[\not{k}/(pk)]u(\vec{p})\delta t$. In our TEM (figure 3), the electron beam travels along the z-axis and the laser orthogonally along y. Furthermore, we choose the polarization of the laser orthogonal to the direction of the electron beam. It follows that $pk = -E_p\omega + \vec{p}\cdot\vec{k} = -E_p\omega$ and

$$\phi = \frac{-e^2\rho\delta t}{2E_p^2\omega^2}\bar{u}(\vec{p})[-\gamma^0\omega+\gamma^2 k]u(\vec{p}) = \frac{\hbar\alpha\rho\lambda\delta t}{\sqrt{m^2+p^2/c^2}}. \quad (2)$$

This agrees with the non-relativistic result if $p/c \ll m$.

If the laser is polarized parallel to the electron beam, $pk = -E_p\omega + p_z k_z$ and $\phi = \lambda\hbar\alpha\rho\delta t/(p_z/c - \sqrt{m^2+p^2/c^2})$. For nonrelativistic electrons, this again reduces to equation (2). In the limit of zero electron velocity, the symmetry for rotation around the wavevector of the laser light means that both polarizations will give rise to the same potential.

We remark that we have treated the laser beam as a plane wave. A focused beam could be described by a superposition of plane waves in the momentum representation. We can treat each of them in the above manner and calculate the combined effect. This will not lead to strong modifications of our results, because (i) even for the strongly focused beams considered below, the major part of the optical power propagates at wavevectors having relatively small angles with the optical axis and (ii) even for arbitrary wavevectors, the phase shift caused is not zero or of opposite sign, ruling out cancelations.

If $\phi \ll 1$, it clearly describes a phase shift: $|f\rangle = (1 + \mathrm{i}\phi)|\mathrm{i}\rangle \approx \mathrm{e}^{\mathrm{i}\phi}|\mathrm{i}\rangle$. To see whether this still holds for large ϕ, we divide the time interval δt into several small ones. Repeated application of the $S^{(2)}$, once for each small interval, shows that $|f\rangle = \mathrm{e}^{\mathrm{i}\phi}|\mathrm{i}\rangle$. This process amounts to summing an infinite series of Feynman diagrams, in which the processes of figures 1(A) and (B) happen 1,2,3, … times. This is valid as long as other processes such as the spontaneous Compton effect remain negligible. This is satisfied in our case: the fraction of electrons that experience spontaneous Compton scattering (and are thus lost for the imaging) per radian of phase shift is given by $r/\phi = \alpha(\upsilon/c)(\lambda_C/\lambda)$. This is about 10^{-8} for $\lambda = 1\mu\mathrm{m}$.

[8] We used $(\vec{p}+\vec{k})^2 - 1 = 2pk$, $\not{\varepsilon}\not{\varepsilon} = \varepsilon^2 = 1$ and $(2\pi)^4\delta^{(4)}(0) \to V\delta t$ [13].

3. Design of the laser phase plate

We now study how this phase shift can be applied for a cw phase contrast TEM. The laser system used for this has to produce a focus small enough so that low spatial frequencies can be resolved. The effective electron optical focal length in our FEI Titan electron microscope is f = 20 mm. This large effective focal length is achieved with a custom-designed relay lens, which magnifies the electron diffraction pattern with minimal increase in the coefficients of chromatic and spherical aberration. At 300 keV, for example, the first zero in the contrast transfer function is still at about 0.35 nm resolution. Applying a phase shift at spatial frequencies down to $1/(2d) = 1/(36\ \text{nm})$ requires a maximal phase-plate radius of the order of $f\lambda_e/(2d) = 20\text{mm}\times 4.2\ \text{pm}/(36\ \text{nm}) = 2.3\mu\text{m}$ at 80 keV, where λ_e is the electron wavelength. At 300 keV ($\lambda_e \approx 2.0$ pm) the required phase-plate radius decreases to 1.1μm. These numbers set the requirement on the focusing of the beam.

A second requirement on the laser system is to generate the desired phase shift, for which a certain power is necessary. To get a sense of how the phase shift scales with wavelength, we express the photon density $\rho = I\lambda/(2\pi\hbar c^2)$ by the intensity I of a laser beam. To express the intensity by the power P of a laser, note that the area of a focus is proportional to λ^2, so that I is proportional to P/λ^2. The time δt it takes for the electron beam to traverse the focus is also proportional to the wavelength. All in all, $\Delta\phi$ is proportional to λ. Such considerations also show that using a smaller focus (produced, e.g., by a lens with a higher numerical aperture) increases the phase shift.

3.1. Near-spherical cavity

Since the phase shift is proportional to the laser wavelength λ, the required laser power can be minimized by using the longest wavelength at which a focus of the required size can be achieved. The smallest focus for a given wavelength is achieved by the TMn01 mode in a spherical resonant cavity [14] shown in figure 2(B). The cavity provides both focusing and resonant enhancement of the intensity: the laser has to supply only the power lost at the cavity walls. The focus has half-intensity radii of 0.25λ and 0.20λ in the x- and y-direction, respectively; the largest intensity maxima other than the focus are less than 10% of the intensity at the focus and can be neglected.

To determine the required laser power, we calculate the energy flow $3E_0^2\pi/(4c\mu_0k^2)$ towards the cavity walls, where E_0 is the peak electric field at the focus, μ_0 is the permeability of free space and k is the laser wavenumber. The electric field in the cavity is known from exact solutions of the Maxwell equations [14]. The cavity walls reflect back most of this, but $P=3(1-r)E_0^2\pi/(4\eta k^2)$, where r is the reflectivity of the cavity walls that is lost and has to be replaced by the laser. Expressing the photon density by the electric field $E_z^2=2\rho\hbar\omega c\mu_0$ (where the factor of 2 accounts for the time averaging of the intensity) and integrating along the z-axis $\int_{-\infty}^{\infty}E_z^2(x=0,y=0,z)\mathrm{d}z=\frac{3}{5}E_0^2\lambda$, we obtain $\phi=\frac{4}{5(1-r)}\frac{\lambda P\alpha}{\gamma c^2 m\upsilon}$, where $\gamma=1/\sqrt{1-\upsilon^2/c^2}$, or

$$\frac{\Delta\phi}{\pi/2}\approx\gamma^{-1}\left(\frac{P}{\mathrm{kW}}\right)\left(\frac{\lambda}{\mu\mathrm{m}}\right)\left(\frac{\upsilon}{c}\right)^{-1}\mathcal{N}, \tag{3}$$

where $\mathcal{N}\approx 0.15/(1-r)$.

Such cavities can use metal coatings for the inner walls. For gold, for example, $r\approx 0.98$ in the infrared. Achieving optimal phase contrast with a cut-on spatial frequency of 1/(40 nm) with a modified FEI Titan electron microscope that is available at Berkeley requires a half-intensity

radius of about 2μm at an electron energy of 80 keV or 1μm at 300 keV. The longest wavelength at which a 2μm focus can be achieved is about λ ~ 10μm. If we choose a CO_2 laser at 10.6μm and let $r = 0.98$ and $\upsilon = c/2$, we need a power of about 7.5W. A 1-μm focus can be achieved using $P = 39$W at λ = 2μm or $P = 75$W at 1064 nm.

For a perfect sphere, all modes with the same radial mode number will resonate at the same frequency. However, of these modes, only the TM*n*01 mode with the lowest angular mode numbers is useful for our purpose, because this mode will result in the electric field distribution shown in figure 2. To help coupling the laser power into the TM*n*01 mode only, distortion of the sphere will lift the degeneracy of modes: the TM*n*01 mode will then have a distinct resonance frequency and can be selected by tuning the laser frequency. Coupling the laser beam into the cavity can be achieved, e.g., via a hole of radius $r_{in}=R\sqrt{2(1-r)/3}$ in the cavity, where R is the radius of the cavity. This radius is determined such that the power lost at the walls balances the one delivered through the hole when the electromagnetic field of the laser matches the resonant field inside the sphere. The laser–cavity coupling efficiency is then given by the overlap integral of the laser and the cavity field. For a Gaussian laser beam, the optimum power transfer is 50.4% and occurs when the $1/e^2$ intensity radius ('waist') of that beam equals the hole radius and a lens of appropriate focal length is used (figure 2(A)). The overlap can be increased by transforming the Gaussian beam into a uniform-intensity beam, which is possible with 84–90% efficiency [15,16]. In order to maintain resonance, the laser frequency can be stabilized to the cavity resonance (or vice versa) using the Pound–Drever–Hall [17] or similar methods.

3.2. Plano-parabolic cavity

A parabolic mirror with radius much larger than focal length produces a focus with an electric field similar to the one in a spherical cavity [18]. Together with a planar partial mirror, a plano-parabolic cavity can be realized, see figure 3. This is easier to manufacture, as no hollow spheres need to be produced. Moreover, the partial mirror is planar or near-planar and can thus have a low-loss dielectric coating. Finally, the laser beam feeding the cavity is collimated, simplifying mode match. The phase shift is given approximately by the same equation as for the sphere, but r is replaced by an effective reflectivity r_{eff}, which is reduced because of losses when the photons spill over the perimeter of the mirror. $r_{eff} = 0.9$ might be possible, and the required laser power is now 35W. Such an arrangement could thus satisfy all requirements using a CO_2 laser.

3.3. Fabry–Perot cavity

Power buildup by factors of 100 000 or more [19] is possible with high-reflectivity dielectric mirrors. Unfortunately, they can at present only be applied to relatively flat surfaces. Cavities using such mirrors are called Fabry–Perot cavities; their eigenmodes are Gaussian beams [20]. In order to keep losses due to the mirror aperture below a part per million, we choose the mirror radius $r_m \gtrsim (5/2)w(L/2)$, where $w(L/2)$ is the $1/e^2$ intensity radius of the beam at the mirrors. This results in a radius $w_0 = (5/2)\lambda/(\pi\mathrm{NA})$ of the focus, where numerical aperture $\mathrm{NA} = r_m/R$. The phase shift is given by equation (3) where the factor $\mathcal{N} = 0.030/(1-r)$.

At present, commercial dielectric mirrors reach NA = 0.04. At λ = 532 nm and a finesse $\mathcal{F} \equiv \pi/(1-r) = 50\,000$, we would thus need a laser power of 8W, which is available from commercial lasers. However, to obtain a 1/2 intensity radius of 2μm, which corresponds to a $1/e^2$ intensity radius of $w_0 = 1.7$μm, a minimum NA = 0.25 is required at λ = 532 nm. If such a cavity could be built with a finesse of 7500, it would reach the required phase shift with an 8W laser. Even then, however, the standing wave in the cavity will have a large number of maxima and minima along the beam direction, forming a phase grating that diffracts the electron beam and is thus undesirable. Also, the half-width of the intensity in the y-direction is given by the Rayleigh

range $z_R \approx \pi\lambda/(2NA)^2$, and is even larger than w_0. These disadvantages are alleviated at high NA ≈ 1, which makes the central maximum dominate.

3.4. Designs without cavity

A simple way to achieve this is using a lens of large NA, see figure 3, not using a cavity. If the aperture of the lens is 3/2 times the waist $w(f)$ at the lens (so that it transmits 99% of the laser power), the resulting radius of the focus is $w_0 \approx \lambda/(2NA)$. The phase shift is given by equation (3) with $\mathcal{N} = 0.048NA$. With an NA of 1, the maximum wavelength in this implementation is about 3μm. Unfortunately, a power of about 4kW would be required even if NA = 1. At λ = 10.6μm with NA = 1, this is reduced to $P = 1.2$kW required, but this results in $w_0 = 5$μm, about three times too large.

In figure 3(C), a standing wave is generated, which has a half-intensity half-width of λ/8 in the beam direction at the cost of a more complicated intensity profile that has several minor peaks. If the focal point of the lens and the mirror coincide, the electric field there is doubled and the intensity quadrupled, resulting in $\mathcal{N} = 0.19NA$. To obtain low spot size in two dimensions, two standing waves can be overlapped as shown in figure 3(D). If these two beams have polarizations orthogonal to the electron beam, and thus orthogonal to each other, their electric fields add geometrically and $\mathcal{N} = 0.19NA$. A similar implementation might use the focused spot as in figure 3(B) and use mirrors to turn the beam 270° and bring it in through a second lens, similar to figure 3(D). We remark that at high NA, the theory of Gaussian beams becomes inaccurate [21]. Depending on the combination of optics and polarization, a factor of safety of 1.2–2 should be applied to the above estimates at NA = 1. This is a further advantage of the spherical or plano-parabolic cavity, where exact analytical expressions have been used to calculate the fields.

4. Applications

At present, the spherical or plano-parabolic cavities appear to be the most promising approaches to construct a cw laser phase plate. Such a phase plate has a number of important advantages over microfabricated ones: since it does not use mechanical structures inside or near the electron beam, it can be completely free of the unwanted electrostatic charging that can occur when electrons hit a solid-phase target, under conventional vacuum conditions. Also, almost none of the electrons that pass through the optical beam are lost, in contrast to thin film or microfabricated phase plates. Moreover, laser phase plates are not subject to the aging experienced by thin carbon-film phase plates [22].

The development of such a reliable phase plate would significantly expand the usefulness of TEMs in biology and in soft-materials science. In current practice, the only option for generating contrast for thin organic materials like biological specimens is to emulate a phase plate by intentionally using a rather large amount of defocus, combined with spherical aberration [23]. Contrast transfer in a defocused TEM image is quite poor, for example, for the low spatial frequencies that carry most of the information about the size, shape and location of an object; it also suffers from contrast reversals (and accompanying zeros) as well as from a damped envelope at higher resolution, when the amount of defocus is increased enough to improve the contrast transfer at low frequencies. By contrast, the laser phase plate would provide full image contrast at low and high resolution at the same time. Use of a quarter-wave phase plate in biology will make it possible to image much smaller protein complexes than can currently be visualized by defocus-based phase contrast, as has been demonstrated with the use of a thin-film phase plate [22]. In most soft-matter applications, the density differences are even smaller than they are for biological materials that are embedded in vitreous ice and thus it is hardly possible to image polymer blends, etc with defocus-based phase contrast. In soft-

matter applications, the use of a quarter-wave phase plate will thus open up greater possibilities for imaging unstained specimens under low-dose conditions.

5. Outlook

As an outlook, the intense three dimensional laser foci generated for this work can also be used as very deep dipole traps for electrons [24] atoms and molecules. Trap depths could be in the range of tens or even hundreds of kelvin, allowing, for example, to trap room-temperature atoms of almost any kind and localize them to better than 0.5μm. This would allow for spectroscopy of exotic species. For example, spectroscopy of the ~ 5–6 eV transition in the thorium 229 nucleus would allow for the construction of clocks based on nuclear energy levels but has so far been thwarted by the lack of a suitable atom trap. The dipole trap proposed here could solve this problem and thus lead to higher precision clocks (as the nucleus of an atom is less sensitive to the environment than the electron shell), tests of the time variability of fundamental constants of unprecedented accuracy, or searches for an electron electric dipole moment [25]. Moreover, a phase contrast TEM could be used for scattering-free quantum nondemolition imaging of atoms, ions or molecules.

Acknowledgments

We thank Eva Nogales for discussions and Mike Hohensee for help in preparing the manuscript. This research was supported by NIH grant GM083039, the David and Lucile Packard Foundation and the Alfred P Sloan Foundation.

References

1. Glaeser, R.; Downing, K.; DeRosier, D.; Chiu, W.; Frank, J. Electron Crystallography of Biological Macromolecules. Oxford: Oxford University Press; 2007. Spence, JCH. High Resolution Electron Microscopy. New York: Oxford University Press; 2003.
2. Zernicke F. Physica 1942;9:686–698.Zernicke F. Physica 1942;9:974–986.Zernicke F. Science 1955;121:345–349. [PubMed: 13237991]
3. Boersch H. Z. Nat.forsch. A 1947;2:615.
4. Hosokawa F, Danev R, Arai Y, Nagayama K. J. Electron Microsc 2005;54:317–324.
5. Nagayama K, Danev R. Phil. Trans. R. Soc. B 2008;363:2153–2162. [PubMed: 18339604]
6. Schultheiß K, Pérez-Willard F, Barton B, Gerthsen D, Schröder RR. Rev. Sci. Instrum 2006;77:033701.
7. Cambie R, et al. Ultramicroscopy 2007;107:329–339. [PubMed: 17079082]
8. Nagayama K, Danev R. Biophys. Rev 2009;1:37–42. [PubMed: 20585379]
9. Danev R, Nagayama K. Ultramicroscopy 2001;88:243–252. [PubMed: 11545320]
10. Volkov DM. Z. Physik 1936;94:250.Dawson JF, Fried Z. Phys. Rev. Lett 1967;19:467.Berestekskii, V.; Lifshitz, EM.; Pitaevskii, LP. Relativistic Quantum Theory. Oxford: Pergamon Press; 1971. p. 122
11. https://ipo.llnl.gov/?q=technologies-phase plate
12. Barwick B, Batelaan H. New J. Phys 2008;10:083036.
13. Mandl, F.; Shaw, G. Quantum Field Theory. New York: Wiley; 1993.
14. Zhang, K.; Li, D. Electromagnetic Theory for Microwaves and Optoelectronics. Berlin: Springer; 2007.
15. Matizen Y, Troitskii YV. Sov. J. Quantum Electron 1989;19:398–402.
16. Palima D, Glückstad J. Opt. Express 2008;16:1507–1516. [PubMed: 18542226]
17. Drever RWP, et al. Appl. Phys. B 1983;31:97–105.
18. Stadler J, Stanciu C, Stupperich C, Meixner AJ. Opt. Lett 2008;33:681–683. [PubMed: 18382516]
19. Hood CJ, Kimble HJ, Ye J. Phys. Rev. A 2001;64 033804.
20. Siegman, AE. Lasers. Sausalito: University Science Books; 1986.

21. Lieb MA, Meixner AJ. Opt. Express 2001;8:458–474. [PubMed: 19417842] Lekner J. J. Opt. A 2003;5:614.Lindfors K, et al. Nature Photonics 1:228.
22. Danev R, Glaser RM, Nagayama K. Ultramicroscopy 2009;109:312–325. [PubMed: 19157711]
23. Lentzen M. Ultramicroscopy 2004;99:211–220. [PubMed: 15149715]
24. Moore CI. J. Mod. Optics 1992;39:2171.
25. Roberts, BL.; Marciano, WJ., editors. Lepton Dipole Moments. Singapore: World Scientific; 2009.

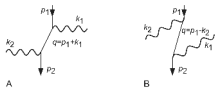

Figure 1.
Feynman diagrams for Compton scattering. p_1, q, and p_2, respectively, denote the initial, intermediate and final momenta of the electron; k_1 and k_2 are the photon momenta.

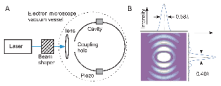

Figure 2.
(A) The setup for a phase contrast TEM using a near-spherical resonant cavity. The electron beam is propagating orthogonal to the paper plane. (B) Intensity of the TM*n*01 mode in a spherical cavity. Shown is a two-dimensional contour plot as well as the intensities along the *x* and *y* axes through the focus, respectively.

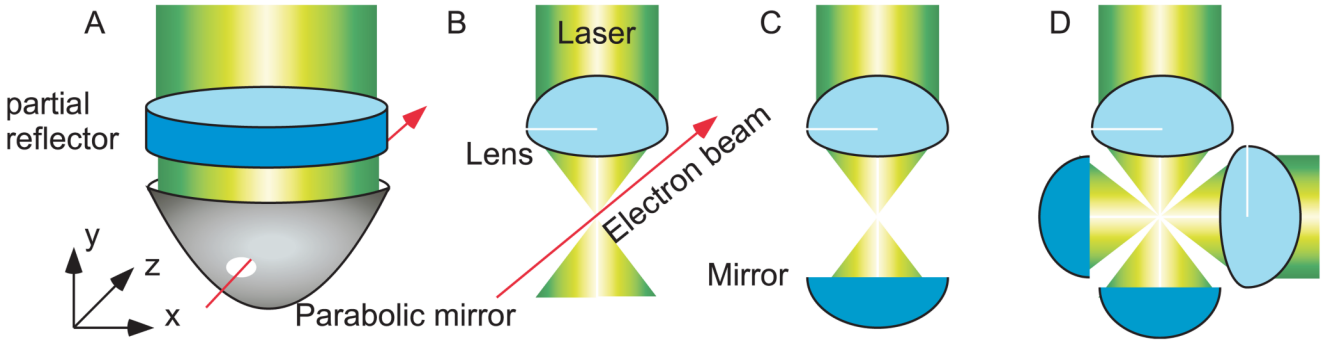

Figure 3.
Alternative realizations of laser phase plates. (A) Plano-parabolic cavity; (B) high-NA lens; (C) high-NA lens with retroreflector; (D) two focused, retroreflected beams. The electron beam is propagating orthogonally to the page.